Using ultrasonic investigations to develop anisotropic damage models for initially transverse isotropic materials undergoing damage to remain transverse isotropic

Louise Olsen-Kettle[a]

[a]*Swinburne University of Technology, School of Science, Mathematics Department, Hawthorn Vic 3122, Australia*

Abstract

A severe limitation imposed by many continuum damage mechanics models is the assumption of initial isotropy in many anisotropic damage models. This may place unrealistic assumptions about the material being modelled or restrict the application of continuum damage mechanics to materials without significant anisotropy. It remains a challenge to use anisotropic continuum damage mechanics to model common rocks and materials with significant initial anisotropy, for example sedimentary rocks or brittle composite materials. We show how ultrasonic investigations in experiments where an initially transverse isotropic material undergoes damage-induced anisotropy can be used to guide the development of transverse isotropic damage models. We provide a robust way to validate and advance models of general anisotropic damage evolution based on continuum damage mechanics.

Keywords:
continuum damage mechanics, anisotropy, ultrasonics stiffness reduction, damage tensor

1. Introduction

Modelling and analysis of fracture propagation and progressive damage evolution are integral for damage-tolerant design in manufacturing, mechani-

Email address: lolsenkettle@swin.edu.au (Louise Olsen-Kettle)

cal, structural and civil engineering. Among the various approaches to model fracture and damage in solids, methods of continuum damage mechanics have gained the most attention. Two of the most challenging problems which arise in continuum damage mechanics is firstly the selection of variables to describe the internal damage and secondly the difficulty in modelling materials with significant initial anisotropy (eg. composites, sedimentary rocks). Very few damage models have been proposed for initially anisotropic materials (Cazcu et al. (2007)) and the correct modelling of the interaction of initial anisotropy and damage-induced anisotropy remains a much debated issue (Halm et al. (2002)). This paper outlines a method to identify the directionality and magnitude of the induced anisotropic damage for initially transverse isotropic materials using experimental ultrasonic measurements of damaged elastic moduli. This research provides an interface between theory and experiment, detailing a simple way to experimentally test and verify models of anisotropic damage evolution for initially transverse isotropic materials remaining transverse isotropic with damage. In future work we will extend these results to modelling anisotropic damage for initially transverse isotropic or orthotropic materials becoming orthotropic with damage.

Anisotropy is an important factor in producing composites with optimum utilization of the inherent strengths of the constituent materials. Manufacturing materials with optimum strength properties is important in reducing safety margins and cutting costs. With the rapid advancement in material design, the assumption of scalar isotropic damage may not suffice and more accurate models of anisotropic damage for initially anisotropic materials are needed. This research aims to address some of these challenges by providing a way to develop phenomenological models of anisotropic damage for initially transverse isotropic materials, such as unidirectional fibre reinforced composites or shales, using experimental measurements of ultrasonic elastic wave velocities and the framework of continuum damage mechanics.

Nondestructive testing using ultrasonic investigations is a relatively mature field for composite materials (Castellano et al. (2017); Marguéres and Meraghni (2013); Audoin and Baste (1994); Hufenbach et al. (2006)etc). However the monitoring of elastic wave velocities in anisotropic sedimentary rocks such as shale is relatively uncommon (Sarout et al. (2007); Sarout and Guéguen (2008a); Piane et al. (2015); Kuila et al. (2011); Bonnelye et al. (2017)). This work will not only advance models of anisotropic damage in composites but also can be applied to other quasi-brittle materials with initial transverse isotropy such as sedimentary rocks like shales.

In many geotechnical applications such as unconventional oil and gas extraction, carbon dioxide sequestration, nuclear waste disposal and geothermal energy extraction the initial anisotropy of the rock can impact on the stability of structures such as cavities, wellbores, or hydraulic fractures. Although shales are the dominant clastic component in sedimentary basins, our understanding of their behaviour is very limited and shale anisotropy has been known to be a significant problem for seismic exploration for many years (Dodds et al. (2007)). The elastic anisotropy in shales can amount to up to 50-60% in elastic stiffnesses and shales are often modelled as a transverse isotropic material. Clayrocks, and shales in particular, represent approximately two-third of all sedimentary rocks in shallow earth crustal rocks. In oil and gas drilling operations, shales constitute 80% of all the drilled sections, mainly because they overlie most hydrocarbon bearing reservoirs (Sarout et al. (2007)). Modeling rock damage during the process of hydraulic fracturing is still an open issue and predicting the actual geometry of the crack pattern in the field is challenging especially in anisotropic unconventional reservoirs such as shales and coal seams. The anisotropy of clayrocks and shales is not just important in petroleum and civil engineering but also if they are to be used as possible sites for storing nuclear waste (Guéguen and Kachanov (2011)). This work aims to advance models of anisotropic damage using continuum damage mechanics so that they can be applied to materials with significant initial anisotropy and in this paper we consider initially transverse isotropic materials such as sedimentary rocks or composites.

Several of the challenges in developing anisotropic damage models are firstly to develop anisotropic damage models which can be applied to initially anisotropic materials, secondly to identify the directionality and magnitude of the damage-induced anisotropy, and lastly to perform measurements which test the predictions of the proposed models. We show how anisotropic damage models can be developed for initially transverse isotropic materials remaining transverse isotropic. We provide a quantitative relationship between the macroscopic, empirically observed damaged elastic moduli and the internal damage variables in section 4. We analyze the tensorial damage evolution for four initially transverse isotropic materials undergoing damage to remain transverse isotropic in section 5.

In section 2 we review current approaches to modelling anisotropic damage and how they compare with our approach. We outline our model in section 3 following the approach of Cauvin and Testa (1999a). In section 4 we derive the relationship between the internal damage variables used in

general continuum damage mechanics models and the empirically observed reduction in elastic wave speeds. Section 4 extends the work of Cauvin and Testa (1999a,b); Jarić et al. (2012) to consider initially transverse isotropic solids. Section 4.1 and 4.2 expand the scope of these previous papers to relate the internal damage tensor variables (D) to the empirically observed damage tensor (D_E) defined using the stiffness reduction given from ultrasonic measurements. This relationship can help advance and test the predictions of general continuum damage models. In section 5 we analyze experimental results of several initially transverse isotropic solids undergoing damage-induced anisotropy. We plot the internal damage tensor variables, and also the change in the elastic parameters with damage in Fig. 1-4.

In section 5 we apply the derived quantitative relationship between the macroscopic, empirically observed damaged elastic moduli and the internal damage variables from section 4 to four initially transverse isotropic materials undergoing damage to remain transverse isotropic. First we model the damage-induced anisotropy of two initially transverse isotropic shale specimens (with axis of isotropy in z direction) under triaxial loading with the axial loading in the z direction using the experimental ultrasonic measurements of the elastic wave velocities with increasing axial pressure of Sarout and Guéguen (2008a). Second we model the damage-induced anisotropy due to a low velocity impact to two transverse isotropic composites using the ultrasonic measurements of the elastic wave velocities for the experimental results of Marguéres and Meraghni (2013) and Castellano et al. (2017). Castellano et al. (2017) also subjected the composite to post-fatigue tensile loading.

2. Modelling damage-induced anisotropy for initially transverse isotropic materials

Many different models of damage have been proposed using continuum damage mechanics since its inception. Many different mathematical representations for the internal damage variable have been proposed from scalar (Lemaitre (1996); Voyiadjis and Kattan (2012); Zhu and Tang (2004) etc); to second order tensors (Chow and Wang (1987); Murakami (1988); Chaboche (1993)) etc; to fourth order tensors (Ju (1990); Cauvin and Testa (1999a,b); Chaboche (1993)) etc. Scalar damage models are restricted to modelling isotropic damage only and have a further restriction that Poisson's ratio of the material does not change with damage. This restriction may not be

physically realistic as we will show in our analysis of experimental results of anisotropic materials where Poisson's ratio changes significantly in some cases. Second-order tensorial anisotropic damage representation is restrictive compared to fourth-order tensorial formulation, but since its interpretation is quite simple it has been widely used for either metallic or quasi-brittle materials. In this paper we consider the most general case to represent anisotropic damage using a fourth order damage tensor.

Several micromechanical approaches have been employed including effective medium theory (Sarout and Guéguen (2008b); Guéguen and Kachanov (2011); Sayers and Kachanov (1995)) etc and microplane models (Caner and Bažant (2013); Bažant (1984); Bažant and Caner (2005); Yang and Leng (2014)) etc, to model the progressive degradation of anisotropic and isotropic materials. Fabric tensors have also been related to the damage tensor in the work of (Voyiadjis and Kattan (2006, 2009)). We present an alternative phenomenological approach based on ultrasonic elastic wave velocity measurements and continuum damage mechanics. Instead of modelling the various damage mechanisms at the microscale level, we represent the damage indirectly by modelling the average material degradation at the mesoscale for an initially transverse isotropic material undergoing damage-induced anisotropy to remain transverse isotropic. Future work will extend upon these models of transverse isotropic damage resulting from well-defined and constrained loading experiments which result in transverse isotropic damage at both the meso and macroscale level to modelling localized damage at the mesoscale level.

We show how ultrasonic measurements of seismic wave velocities can be used to determine the evolution of the fourth order anisotropic damage tensor characterizing this internal damage. Elastic properties can be determined by static measurements of stress and strain or by dynamic methods such as ultrasonic measurements of the seismic wave velocities (Paterson and Wong (2005)). Ultrasonic methods have been very popular in nondestructive testing and characterization of materials and monitoring progressive damage.

Ultrasonic techniques provide fast and non-destructive methods for reliable measurement of elastic properties and their change with damage (Marguéres and Meraghni (2013)). Ultrasonic techniques have been employed by several researchers (see for example Audoin and Baste (1994); Hufenbach et al. (2006); Castellano et al. (2017)) to identify purely phenomenological models of anisotropic damage for composite materials. Our approach extends these models to equate the phenomenological models of experimentally measured

stiffness reduction during loading given by ultrasound measurements to general fourth order anisotropic damage tensorial models given by continuum damage mechanics in section 3. In section 3 we define the general fourth order anisotropic internal damage tensor using the approach by Cauvin and Testa (1999a) using the principle of strain equivalence and effective stress.

Mallet et al. (2013, 2014) have also investigated cracking using ultrasonic elastic wave velocity and thin section measurements of an initially isotropic glass sample undergoing thermal cracking to become transverse isotropic. Mallet et al. (2013) showed using effective medium theory and the non-interaction approximation (Sayers and Kachanov (1995)) how elastic wave velocity measurements can be used to infer crack densities and thus the damaged material stiffness and compliance tensor for thermally cracked glass. Closed form results for damage induced anisotropy in initially anisotropic materials are available for 2D problems using micromechanical approaches (Guéguen and Kachanov (2011)), however for 3D damage it is much more difficult. Sarout and Guéguen (2008b) have obtained an exact solution for a transverse isotropic rock containing cracks that run parallel to the plane of isotropy. In this paper we also use ultrasonic measurements to quantify the anisotropic 3D damage in a similar approach to these micromechanical approaches. However we relate the ultrasonic measurements to the general internal fourth rank tensorial damage variables defined using continuum damage mechanics for initially transverse isotropic materials undergoing damage-induced anisotropy to remain transverse isotropic.

3. Fourth order damage tensor to characterize the internal damage

Continuum damage mechanics is constructed adopting the following premises: the microstructural changes from damage can be described by means of macroscopic damage variables, the mechanical behavior of a damaged material can be described by a set of constitutive and evolution equations for the state variables. The mechanical formulation of these equations can be performed by the using the notion of effective state variables and the hypothesis of mechanical equivalence between the damaged state and a fictitious undamaged state with equivalent strain or energy (Murakami (2012)). We define the internal damage tensor (D) in this paper to be the damage tensor derived within this continuum damage mechanics framework. We also define an empirical damage tensor (D_E) which represents the reduction of the

elastic stiffness tensor with damage. We quantify the relationship between the empirically measured damage tensor representing the ultrasonics stiffness reduction often employed in purely phenomenological models of damage in composites (see for example Audoin and Baste (1994); Hufenbach et al. (2006); Castellano et al. (2017)) and the internal damage tensor derived using continuum damage mechanics. This relationship allows anisotropic damage models based on continuum damage mechanics to be experimentally validated using this relationship.

In general if we consider a linear relationship between the undamaged and damaged stiffness tensor, then we can define: $\tilde{E} = (I_8 - D_8) :: E$, where $\tilde{E}$ is the damaged stiffness tensor, E is the original undamaged stiffness tensor, I_8 is an eighth rank identity tensor and D_8 is an eighth rank damage tensor. However working with an eighth order tensor description of damage would be very complex. In the seminal work of Cauvin and Testa (1999a) they showed using the principle of strain equivalence that in general only a fourth order damage tensor (D) is needed to describe a material (anisotropic or isotropic) undergoing damage where $\tilde{E} = (I_4 - D) :: E$. Using the framework of continuum damage mechanics and the concept of effective stress and the principle of equivalent strain we follow the approach of Cauvin and Testa (1999a) to define the internal general fourth order damage tensor. We will briefly outline this approach here.

Cauvin and Testa (1999a) used the hypothesis of strain equivalence and the concept of effective stress to define the inelastic constitutive equation of a damaged material. The principle of strain equivalence considers two configurations with equivalent strain. In the damaged configuration where $\sigma = \tilde{E} : E$, σ is the actual stress tensor and E the strain tensor. In the fictitious undamaged configuration where $\tilde{\sigma} = E : \mathbb{E}$, $\tilde{\sigma}$ is the effective stress tensor applied to the undamaged original material to produce the same elastic strain tensor. Because the same elastic strain is considered in both damaged and undamaged materials that strain is considered to be the equivalent strain. Using this principle of strain equivalence Cauvin and Testa (1999a) showed that the most general damage description will reduce from an eighth to a fourth order damage tensor. We use this definition of the general fourth order internal damage tensor (D) defined by Cauvin and Testa (1999a) using continuum damage mechanics: $\tilde{E} = (I_4 - D) :: E$. This is different to our definition of the empirical damage tensor D_E which represents the reduction of the elastic stiffness tensor with damage: $D_{E_{ij}} = 1 - \tilde{E}_{ij}/E_{ij}$ (no summation implied over repeated indice here). However it is clear that the two damage

tensors are related to each other and in this paper we derive this relationship. This provides a way to experimentally validate and guide the development of continuum damage models for transverse isotropic damage that model the damage response of all 5 independent elastic parameters.

Continuum damage mechanics can be used to define the evolution of the internal damage tensor *a priori* using irreversible thermodynamics. This work provides a bridge between this theoretical approach to modelling damage and experimental measurements of stiffness reduction with damage. The relationship between the empirically measured damage tensor (D_E) and the internal damage tensor (D) in sections 4.1 and 4.2 provides a way to independently validate and test existing theoretical anisotropic continuum damage models using ultrasonic measurements.

Cauvin and Testa (1999a) also showed that the actual number of independent damage parameters in the fourth order damage tensor is related to the material and damage symmetry. Cauvin and Testa (1999a) and Jarić et al. (2012) showed that the general supersymmetry requirements for the damaged elastic stiffness tensor $\tilde{E}$ requires that $\tilde{E}_{ijkl} = \tilde{E}_{jikl} = \tilde{E}_{ijlk} = \tilde{E}_{klij}$, and this requirement places the following constraint on the damage tensor:

$$D_{ijrs}E_{rskl} - D_{klrs}E_{rsij} = 0, \tag{1}$$

$$\text{where } \tilde{E}_{ijkl} = (I_{ijrs} - D_{ijrs})E_{rskl}, \tag{2}$$

$$\text{and } I_{ijrs} = \frac{1}{2}(\delta_{ir}\delta_{js} + \delta_{is}\delta_{jr}).$$

where D is the damage tensor, $\tilde{E}$ is the damaged stiffness tensor, E is the original undamaged stiffness tensor and δ_{ij} is the Kronecker delta function. Here we note that the damage tensor is not supersymmetric like $\tilde{E}$ but it does have the same number of independent variables as $\tilde{E}$ (Jarić et al. (2012)). Because E is supersymmetric equation (1) implies that D possesses minor symmetries: $D_{ijkl} = D_{jikl} = D_{ijlk}$. The above equations hold for any material symmetry of the initially undamaged and damaged material. Here we note that we don't need to require that our damage tensor is supersymmetric and that the constraint in equation 1 will ensure that the damaged stiffness tensor remains supersymmetric.

This paper extends the work of Cauvin and Testa (1999a,b) and Jarić et al. (2012) to consider the evolution of the anisotropic damage tensor for initially transverse isotropic materials. Cauvin and Testa (1999a) defined the internal fourth order anisotropic damage tensor for initially isotropic

materials undergoing both isotropic or anisotropic damage. We extend this work to consider initially transverse isotropic materials undergoing damage to remain transverse isotropic. In our previous paper (Olsen-Kettle (2018)) we considered initially isotropic solids undergoing damage to become transverse isotropic.

Jarić et al. (2012) also defined the internal damage tensor for initially isotropic (initially 2 independent elastic parameters) or cubic (initially 3 independent elastic parameters) solids undergoing either isotropic or anisotropic damage. We extend their work to consider initially transverse isotropic materials (5 independent elastic parameters) undergoing transverse isotropic damage. Furthermore we expand on the analysis of Jarić et al. (2012) to relate the fourth order internal damage tensor variables to the empirically measurable reduction in the stiffness tensor of initially transverse isotropic materials undergoing anisotropic damage.

Cauvin and Testa (1999a,b) relate the change in well-known elastic parameters, such as the bulk modulus, Young's modulus and Poisson's ratio with damage, to the internal damage variables for the case of an initially isotropic solid undergoing damage to remain isotropic. We extend this approach to consider initially transverse isotropic solids undergoing damage to remain transverse isotropic. We employ different empirical measures of damage to Cauvin and Testa (1999a,b). Cauvin and Testa (1999a,b) relate the internal fourth order damage tensor variables to the change in isotropic elastic moduli and Poisson's ratio with damage. Because we are considering initially anisotropic materials and the evolution of anisotropic damage we use a more convenient empirical measure of damage which is the experimentally measured stiffness reduction using ultrasonic investigations. We chose this measure of damage as ultrasonic investigations are widely used in many anisotropic materials such as composites, and provide a convenient experimental tool to measure the evolution of the full stiffness tensor. The evolution of the full stiffness tensor is required to consider anisotropic damage evolution.

Here we note that we use the conventional definition of the damage tensor using continuum damage mechanics defined as: $\tilde{E} = (I - D) : E$ in equation 2 using the double inner product instead of a new definition of the damage tensor used by Audoin and Baste (1994); Hufenbach et al. (2006); Castellano et al. (2017). Audoin and Baste (1994) defined the damage tensor used in these references using an additive form where: $\tilde{E} = E - E_d$ and E_d is their damage tensor before normalization. The damage tensor used in these

models is similar to our definition for the empirical damage tensor D_E.

4. Damage induced anisotropy in initially transverse isotropic materials

The compliance tensor in Voigt notation for an initially transverse isotropic material with the axis of isotropy in the z direction is:

$$S = \begin{bmatrix} \frac{1}{E} & \frac{-\nu}{E} & \frac{-\nu^t}{E^t} & 0 & 0 & 0 \\ \frac{-\nu}{E} & \frac{1}{E} & \frac{-\nu^t}{E^t} & 0 & 0 & 0 \\ \frac{-\nu^t}{E^t} & \frac{-\nu^t}{E^t} & \frac{1}{E^t} & 0 & 0 & 0 \\ 0 & 0 & 0 & \frac{1}{G^t} & 0 & 0 \\ 0 & 0 & 0 & 0 & \frac{1}{G^t} & 0 \\ 0 & 0 & 0 & 0 & 0 & \frac{2(1+\nu)}{E} \end{bmatrix}$$

where $E = E_x = E_y$ is the Young's modulus in directions x and y, $E^t = E_z$ is the Young's modulus in the z direction; $G^t = G_{yz} = G_{xz}$ is the shear modulus for coordinate planes y-z and x-z; and $\nu^t = \nu_{zy} = \nu_{zx}$ and $\nu = \nu_{yx} (= \nu_{xy})$ are the Poisson's ratios in the direction of the second subscript produced by a load in the direction of the first subscript. Here we note that Poisson's ratios are not symmetric (i.e. $\nu_{ij} = \nu_{ji}$ however they do satisfy $\nu_{ij}/E_i = \nu_{ji}/E_j$.

The stiffness tensor for the initially transverse isotropic material E is simply the inverse of the compliance tensor:

$$E = S^{-1} = \begin{bmatrix} \frac{E(E^t - E\nu^{t2})}{(1+\nu)[(1-\nu)E^t - 2E\nu^{t2}]} & \frac{E(\nu E^t + E\nu^{t2})}{(1+\nu)[(1-\nu)E^t - 2E\nu^{t2}]} & \frac{EE^t\nu^t}{[(1-\nu)E^t - 2E\nu^{t2}]} & 0 & 0 & 0 \\ \frac{E(\nu E^t + E\nu^{t2})}{(1+\nu)[(1-\nu)E^t - 2E\nu^{t2}]} & \frac{E(E^t - E\nu^{t2})}{(1+\nu)[(1-\nu)E^t - 2E\nu^{t2}]} & \frac{EE^t\nu^t}{[(1-\nu)E^t - 2E\nu^{t2}]} & 0 & 0 & 0 \\ \frac{EE^t\nu^t}{[(1-\nu)E^t - 2E\nu^{t2}]} & \frac{EE^t\nu^t}{[(1-\nu)E^t - 2E\nu^{t2}]} & \frac{(1-\nu)E^{t2}}{[(1-\nu)E^t - 2E\nu^{t2}]} & 0 & 0 & 0 \\ 0 & 0 & 0 & G^t & 0 & 0 \\ 0 & 0 & 0 & 0 & G^t & 0 \\ 0 & 0 & 0 & 0 & 0 & \frac{E}{2(1+\nu)} \end{bmatrix},$$

$$= \begin{bmatrix} E_{11} & E_{12} & E_{13} & 0 & 0 & 0 \\ E_{12} & E_{11} & E_{13} & 0 & 0 & 0 \\ E_{13} & E_{33} & 0 & 0 & 0 & \\ 0 & 0 & E_{44} & 0 & 0 & \\ 0 & 0 & 0 & E_{44} & 0 & \\ 0 & 0 & 0 & 0 & E_{66} & \end{bmatrix}$$

$$= \begin{bmatrix} E_{13} \\ 0 \\ 0 \end{bmatrix}$$

Here we are using Voigt notation where each pair of indices (ij and kl) is replaced by a single index: $11 \rightarrow 1$, $22 \rightarrow 2$, $33 \rightarrow 3$, $23, 32 \rightarrow 4$, $13, 31 \rightarrow 5$, and $12, 21 \rightarrow 6$.

For this paper we assume that the material symmetry axes of the transverse isotropic solid do not change and we apply our analysis to the experimental loading conditions of Sarout and Guéguen (2008a); Marguéres and Meraghni (2013) and Castellano et al. (2017). These authors showed using ultrasonic investigations that this assumption is valid. Thus when deriving the stiffness tensor for the damaged material $\tilde{E}$ and the damage tensor D we use the material axes of the original undamaged initial transverse isotropic specimens as the material axes for the damaged transverse isotropic specimens. Future work will also investigate the case of off-axis loading where the material axes and the principal stress directions do not align as in the experiments of Baste and Aristiégui (1998).

The stiffness tensor for the damaged material remaining transverse isotropic with the same material symmetry axes (again using the material axes of the

initial undamaged transverse isotropic material) in Voigt notation is:

$$\tilde{E} = \begin{bmatrix} \frac{\tilde{E}(\tilde{E}^l - \tilde{E}\tilde{\nu}^{l2})}{(1+\tilde{\nu})[(1-\tilde{\nu})\tilde{E}^l - 2\tilde{E}\tilde{\nu}^{l2}]} & \frac{\tilde{E}(\tilde{\nu}\tilde{E}^l + \tilde{E}\tilde{\nu}^{l2})}{(1+\tilde{\nu})[(1-\tilde{\nu})\tilde{E}^l - 2\tilde{E}\tilde{\nu}^{l2}]} & \frac{\tilde{E}\tilde{E}^l\tilde{\nu}^l}{[(1-\tilde{\nu})\tilde{E}^l - 2\tilde{E}\tilde{\nu}^{l2}]} & 0 & 0 & 0 \\ \frac{\tilde{E}(\tilde{\nu}\tilde{E}^l + \tilde{E}\tilde{\nu}^{l2})}{(1+\tilde{\nu})[(1-\tilde{\nu})\tilde{E}^l - 2\tilde{E}\tilde{\nu}^{l2}]} & \frac{\tilde{E}(\tilde{E}^l - \tilde{E}\tilde{\nu}^{l2})}{(1+\tilde{\nu})[(1-\tilde{\nu})\tilde{E}^l - 2\tilde{E}\tilde{\nu}^{l2}]} & \frac{\tilde{E}\tilde{E}^l\tilde{\nu}^l}{[(1-\tilde{\nu})\tilde{E}^l - 2\tilde{E}\tilde{\nu}^{l2}]} & 0 & 0 & 0 \\ \frac{\tilde{E}\tilde{E}^l\tilde{\nu}^l}{[(1-\tilde{\nu})\tilde{E}^l - 2\tilde{E}\tilde{\nu}^{l2}]} & \frac{\tilde{E}\tilde{E}^l\tilde{\nu}^l}{(1-\tilde{\nu})\tilde{E}^l - 2\tilde{E}\tilde{\nu}^{l2}} & \frac{(1-\tilde{\nu})\tilde{E}^{l2}}{[(1-\tilde{\nu})\tilde{E}^l - 2\tilde{E}\tilde{\nu}^{l2}]} & 0 & 0 & 0 \\ 0 & 0 & 0 & \tilde{G}^t & 0 & 0 \\ 0 & 0 & 0 & 0 & G & 0 \\ 0 & 0 & 0 & 0 & 0 & \frac{\tilde{E}}{2(1+\tilde{\nu})} \end{bmatrix},$$

$$= \begin{bmatrix} \tilde{E}_{11} & \tilde{E}_{12} & \tilde{E}_{13} & 0 & 0 & 0 \\ \tilde{E}_{12} & \tilde{E}_{11} & \tilde{E}_{13} & 0 & 0 & 0 \\ \tilde{E}_{13} & \tilde{E}_{13} & \tilde{E}_{33} & 0 & 0 & 0 \\ 0 & 0 & 0 & \tilde{E}_{44} & 0 & 0 \\ 0 & 0 & 0 & 0 & \tilde{E}_{44} & 0 \\ 0 & 0 & 0 & 0 & 0 & \tilde{E}_{66} \end{bmatrix},$$

$$= \begin{bmatrix} \tilde{E}_{1111} & \tilde{E}_{1122} & \tilde{E}_{1133} & 0 & 0 & 0 \\ \tilde{E}_{1122} & \tilde{E}_{2222} & \tilde{E}_{2233} & 0 & 0 & 0 \\ \tilde{E}_{1133} & \tilde{E}_{2233} & \tilde{E}_{3333} & 0 & 0 & 0 \\ 0 & 0 & 0 & \tilde{E}_{2323} & 0 & 0 \\ 0 & 0 & 0 & 0 & \tilde{E}_{1313} & 0 \\ 0 & 0 & 0 & 0 & 0 & \tilde{E}_{1212} \end{bmatrix}.$$

where $\tilde{E}_{12} = \tilde{E}_{11} - 2\tilde{E}_{66}$, $\tilde{E} = \tilde{E}_x = \tilde{E}_y$ is the damaged Young's modulus in directions x and y, $\tilde{E}^t = \tilde{E}_z$ is the damaged Young's modulus in the z direction; $\tilde{G}^t = \tilde{G}_{yz} = \tilde{G}_{xz}$ is the damaged shear modulus for coordinate planes y-z and x-z; and $\tilde{\nu}^t = \tilde{\nu}_{zy} = \tilde{\nu}_{zx}$ and $\tilde{\nu} = \tilde{\nu}_{yx} (= \tilde{\nu}_{xy})$ are the damaged Poisson's ratio in the direction of the second subscript produced by a load in the direction of the first subscript. Here we note that Poisson's ratios are not symmetric (i.e. $\tilde{\nu}_{ij} \neq \tilde{\nu}_{ji}$ however they do satisfy $\tilde{\nu}_{ij}/\tilde{E}_i = \tilde{\nu}_{ji}/\tilde{E}_j$.

The corresponding general anisotropic damage tensor for a material un-

dergoing transverse isotropic damage can be written in Voigt notation as:

$$D = \begin{bmatrix} D_{11} & D_{12} & D_{13} & 0 & 0 & 0 \\ D_{21} & D_{22} & D_{23} & 0 & 0 & 0 \\ D_{31} & D_{32} & D_{33} & 0 & 0 & 0 \\ 0 & 0 & 0 & D_{44} & 0 & 0 \\ 0 & 0 & 0 & 0 & D_{55} & 0 \\ 0 & 0 & 0 & 0 & 0 & D_{66} \end{bmatrix},$$

$$= \begin{bmatrix} D_{1111} & D_{1122} & D_{1133} & 0 & 0 & 0 \\ D_{2211} & D_{2222} & D_{2233} & 0 & 0 & 0 \\ D_{3311} & D_{3322} & D_{3333} & 0 & 0 & 0 \\ 0 & 0 & 0 & D_{2323} & 0 & 0 \\ 0 & 0 & 0 & 0 & D_{1313} & 0 \\ 0 & 0 & 0 & 0 & 0 & D_{1212} \end{bmatrix}.$$

We can still write D in Voigt notation as equation 1 implies that D possesses the minor symmetries: $D_{ijkl} = D_{jikl} = D_{ijlk}$. Here we note that D is not supersymmetric like $\tilde{E}$. However D still has the same number of independent components (nine) as $\tilde{E}$, and D_{21}, D_{31} and D_{32} are given by the supersymmetric constraint for $\tilde{E}$ (equation 1):

$$\begin{aligned} D_{21} &= \frac{1}{E_{11}}\left((D_{11} - D_{22})E_{12} + (D_{13} - D_{23})E_{13}\right) + D_{12}, \\ D_{31} &= \frac{1}{E_{11}}\left(D_{13}E_{33} + (D_{11} + D_{12} - D_{33})E_{13} - D_{32}E_{12}\right), \\ D_{32} &= \frac{1}{E_{11}}\left(D_{23}E_{33} + (D_{21} + D_{22} - D_{33})E_{13} - D_{31}E_{12}\right). \end{aligned} \qquad (3)$$

Using equation 2 the damaged stiffness tensor variables for $\tilde{E}$ become:

$$\begin{aligned}
\tilde{E}_{11} &= E_{11}(1 - D_{11}) - E_{12}D_{12} - E_{13}D_{13} \\
\tilde{E}_{12} &= -E_{11}D_{12} + E_{12}(1 - D_{11}) - E_{13}D_{13} \\
\tilde{E}_{13} &= -E_{33}D_{13} + E_{13}(1 - D_{11} - D_{12}) \\
\tilde{E}_{22} &= E_{11}(1 - D_{22}) - E_{12}D_{21} - E_{13}D_{23} \\
\tilde{E}_{23} &= -E_{33}D_{23} + E_{13}(1 - D_{21} - D_{22}) \\
\tilde{E}_{33} &= E_{33}(1 - D_{33}) - E_{13}(D_{31} + D_{32}) \\
\tilde{E}_{44} &= G(1 - 2D_{44}) \\
\tilde{E}_{55} &= G(1 - 2D_{55}) \\
\tilde{E}_{66} &= \frac{E(1 - 2D_{66})}{2(1 + \nu)}.
\end{aligned} \tag{4}$$

In the next section we show the conditions for the ultrasonic measurements required for the material to remain transverse isotropic with damage.

4.1. Relating empirical damage parameters to ultrasonic measurements

In this section we define the empirical damage tensor, $D_{E_{ij}}$ which can be experimentally measured. We will define the relationship between the experimentally measured empirical damage tensor (D_E) and the internal damage tensor (D) defined using continuum damage mechanics.

We can define empirical damage variables ($D_{E_{ij}}$) as in Olsen-Kettle (2018) which satisfy $\tilde{E}_{ij} = (1 - D_{E_{ij}})E_{ij}$ (no summation over i, j) to compare the measured decrease in ultrasonic elastic wave velocities (and decrease in corresponding stiffness tensor elements $\tilde{E}_{ij}$) with the internal damage variables (D_{ij}). For example $D_{E_{11}}$ satisfies:

$$\begin{aligned}
\tilde{E}_{11} &= (1 - D_{E_{11}})E_{11}, \\
\text{using equation 4: } \tilde{E}_{11} &= E_{11}(1 - D_{11}) - E_{12}D_{12} - E_{13}D_{13}. \\
\text{Rearranging for } D_{E_{11}}\text{: } D_{E_{11}} &= \frac{1}{E_{11}}(E_{12}D_{12} + E_{13}D_{13}) + D_{11}, \\
\text{and } D_{E_{11}} &= 1 - \frac{\tilde{E}_{11}}{E^{11}}.
\end{aligned}$$

Here we note that the empirical damage parameters are not exactly the same as those used by Baste and Aristiégui (1998); Marguéres and Meraghni (2013) and Castellano et al. (2017). We do not need to symmetrize our

empirical damage tensor to recover a supersymmetric elastic tensor (Olsen-Kettle (2018)). This powerful analysis provides a relationship between experimentally measured empirical damage parameters and the internal fourth order tensorial damage variables using continuum damage mechanics for anisotropic damage of an initially transverse isotropic solid.

Similarly $\tilde{E}_{12} = (1 - D_{E_{12}})E_{12}$ etc and we can rearrange equation 4 to define the empirical damage parameters below:

$$
\begin{aligned}
D_{E_{11}} &= \frac{1}{E_{11}}(E_{12}D_{12} + E_{13}D_{13}) + D_{11} = 1 - \frac{\tilde{E}_{11}}{E^{11}}, \\
D_{E_{22}} &= \frac{1}{E_{11}}(E_{12}D_{21} + E_{13}D_{23}) + D_{22} = 1 - \frac{\tilde{E}_{11}}{E^{11}}, \\
D_{E_{33}} &= \frac{E_{13}}{E_{33}}(D_{31} + D_{32}) + D_{33} = 1 - \frac{\tilde{E}_{33}}{E^{33}}, \\
D_{E_{12}} &= D_{11} + \frac{1}{E_{12}}(E_{11}D_{12} + E_{13}D_{13}) \\
&= 1 + (D_{E_{11}} - 1)\frac{E_{11}}{E_{12}} + 2(1 - D_{E_{66}})\frac{E_{66}}{E_{12}}, \\
&\quad \text{using } \tilde{E}_{12} = \tilde{E}_{11} - 2\tilde{E}_{66}, \\
D_{E_{13}} &= \frac{E_{33}}{E_{13}}D_{13} + D_{11} + D_{12} = 1 - \frac{\tilde{E}_{13}}{E^{13}}, \\
D_{E_{23}} &= \frac{E_{33}}{E_{13}}D_{23} + D_{21} + D_{22} = 1 - \frac{\tilde{E}_{13}}{E^{13}}, \\
D_{E_{44}} &= 2D_{44} = 1 - \frac{\tilde{E}_{44}}{E^{44}}, \\
D_{E_{55}} &= 2D_{55} = 1 - \frac{\tilde{E}_{44}}{E^{44}}, \\
D_{E_{66}} &= 2D_{66} = 1 - \frac{\tilde{E}_{66}}{E^{66}}.
\end{aligned}
\tag{5}
$$

Because the material remains transverse isotropic under loading we have used the fact that $\tilde{E}_{11} = \tilde{E}_{22}$, $\tilde{E}_{13} = \tilde{E}_{23}$ and $\tilde{E}_{44} = \tilde{E}_{55}$. This means that $D_{E_{11}} = D_{E_{22}}$, $D_{E_{13}} = D_{E_{23}}$, and $D_{E_{44}} = D_{E_{55}}$, and we will show in section 4.2 that this implies that $D_{11} = D_{22}$, $D_{13} = D_{23}$, $D_{12} = D_{21}$ $D_{31} = D_{32}$, and $D_{44} = D_{55}$.

4.2. *Quantifying internal damage variables of a fourth rank transverse isotropic damage tensor in terms of the empirical damage parameters given by ultrasonic measurements*

To relate the internal fourth rank damage variables (D_{ij}) to the empirical damage variables ($D_{E_{ij}}$) we can invert equations 5 and use the constraints for D_{21}, D_{31} and D_{32} in equation 3. The internal damage variables are:

$$D_{11} = D_{22} = \frac{(\upsilon-1)E^t[D_{E_{11}} + \upsilon D_{E_{66}}] + E\upsilon_2^t[(1-\upsilon)D_{E_{11}} + (1+\upsilon)D_{E_{13}} + 2\upsilon D_{E_{66}}]}{(1+\upsilon)[(\upsilon-1)E^t + 2E\upsilon^{t2}]},$$

$$D_{13} = D_{23} = \frac{-E\upsilon^t\{2E\upsilon^{t2}(D_{E_{11}} - D_{E_{66}}) + E^t[-2D_{E_{11}} + (1+\upsilon)D_{E_{13}} + (1-\upsilon)D_{E_{66}}]\}}{(1+\upsilon)E^t[(\upsilon-1)E^t + 2E\upsilon^{t2}]},$$

$$D_{12} = D_{21} = \frac{E\upsilon^{t2}[(1-\upsilon)D_{E_{11}} + (1+\upsilon)D_{E_{13}} - 2D_{E_{66}}] + E^t(\upsilon-1)(D_{E_{11}} - D_{E_{66}})}{(1+\upsilon)[(\upsilon-1)E^t + 2E\upsilon^{t2}]},$$

$$D_{33} = \frac{2E\upsilon^{t2}D_{E_{13}} + E^t(\upsilon-1)D_{E_{33}}}{(\upsilon-1)E^t + 2E\upsilon^{t2}},$$

$$D_{31} = D_{32} = \frac{E^t\upsilon^t(\upsilon-1)[D_{E_{13}} - D_{E_{33}}]}{(\upsilon-1)E^t + 2E\upsilon^{t2}},$$

$$D_{44} = D_{55} = \frac{D_{E_{44}}}{2},$$

$$D_{66} = \frac{D_{E_{66}}}{2},$$

where $D_{E_{11}}, D_{E_{13}}, D_{E_{33}}, D_{E_{44}}$ and $D_{E_{66}}$ are measured experimentally from the ultrasonic elastic wave measurements.

In this paper we only consider experiments where the principal applied stresses are coaxial with the material axes of the original transverse isotropic material and the damaged material. We consider a change in the magnitude of the initial anisotropy with damage but no change in the material axes' directions with damage for this paper.

The fourth order damage tensor for an initially transverse isotropic solid undergoing damage to become transverse isotropic (where the material symmetry axes do not change from undamaged to damaged state) in Voigt no-

tation is:

$$D = \begin{bmatrix} D_{11} & D_{12} & D_{13} & 0 & 0 & 0 \\ D_{12} & D_{11} & D_{13} & 0 & 0 & 0 \\ D_{31} & D_{31} & D_{33} & 0 & 0 & 0 \\ 0 & 0 & 0 & D_{44} & 0 & 0 \\ 0 & 0 & 0 & 0 & D_{44} & 0 \\ 0 & 0 & 0 & 0 & 0 & D_{66} \end{bmatrix}$$

5. Internal damage variables for experiments of damage-induced anisotropy in initially transverse isotropic solids

Figures 1 to 4 analyze the ultrasonic elastic velocity measurements of Sarout and Guéguen (2008a); Marguéres and Meraghni (2013) and Castellano et al. (2017) and relate them to internal damage tensor variables for different transverse isotropic materials undergoing damage-induced anisotropy to remain transverse isotropic. All the materials are initially transverse isotropic with the axis of isotropy in the z direction. Sarout and Guéguen (2008a) investigated stress-induced anisotropy of both a wet and dry shale sample undergoing triaxial loading with axial loading perpendicular to the bedding plane (plane of isotropy). Castellano et al. (2017) considered a low-velocity impact in the x direction followed by fatigue tensile loading in the z direction for a glass fibre-reinforced composite. Marguéres and Meraghni (2013) consider a low velocity impact in the z direction for a polyester composite.

5.1. Damage-induced anisotropy in shale samples

Sarout and Guéguen (2008a) investigated stress-induced anisotropy of both a wet and dry shale sample undergoing triaxial loading with axial loading perpendicular to the bedding plane (plane of isotropy). The authors obtained samples from the same core a few cms apart and cored the samples perpendicular to the bedding plane. The dry shale sample was dried at 105°C, while the wet shale sample was equilibrated in an atmosphere of 98% relative humidity. As noted by Sarout and Guéguen (2008b) interpretation of the wet experiment is less straightforward, and we add to their interpretation and analysis of their experimental results. The presence of water in the shale's crack-like pore network has the most effect on Poisson's ratio as we can observe in the difference in Poisson's ratio when comparing the dry shale sample's elastic moduli in Table 1 at room temperature with the respective wet shale sample's elastic moduli in Table 2.

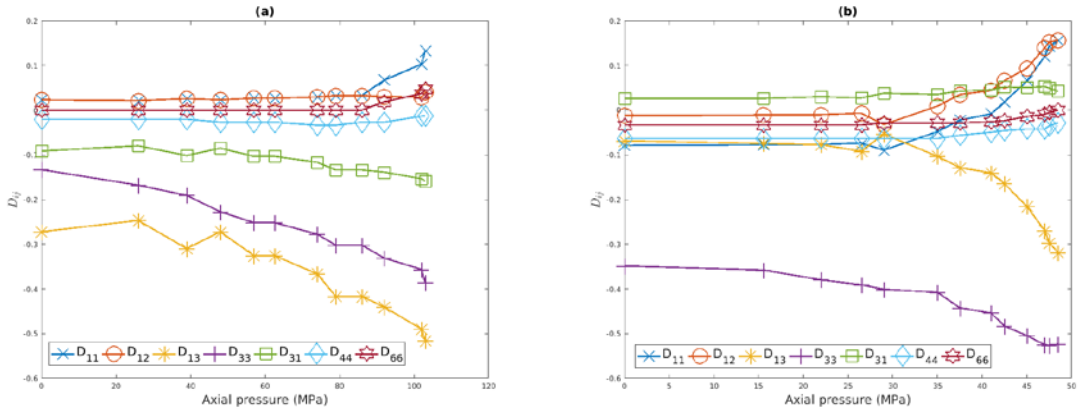

Figure 1: The internal tensorial damage variables for a dry (a) and wet (b) shale rock specimen under triaxial loading with a confining pressure of 15MPa for the experimental results of Sarout and Guéguen (2008a) (see Fig. 14). Their experimental results showed a change in the elastic moduli but not in the material axes of symmetry with the axis of isotropy remaining in the z direction.

The internal damage tensor variable is plotted in Fig. 1 as a function of increasing axial stress until peak stress is reached and rupture along a shear plane occurs for the experimental results of Sarout and Guéguen (2008a) (see Sarout and Guéguen (2008a), Fig. 14). Figures 1 and 2 consider the experiments of Sarout and Guéguen (2008a) for the second axial loading of the dry and wet shale samples with a constant confining pressure of 15MPa. The wet sample was loaded far beyond peak stress, however the dry sample was only loaded to peak axial stress. In Fig. 1 we consider negative values of the damage which correspond to strain hardening due to microcrack closure during the triaxial loading and we observe that some of the damage is reversible. Negative values of the internal damage variables were also observed by Castellano et al. (2017) and they also noted that this does not violate any theoretical assumptions on the damage tensor. Perhaps in future work it could be advantageous to also consider an additional healing tensorial variable to represent the strain hardening behavior.

Fig. 1 plots the internal tensorial damage variables for a shale rock specimen under triaxial loading with a confining pressure of 15MPa for the ex-

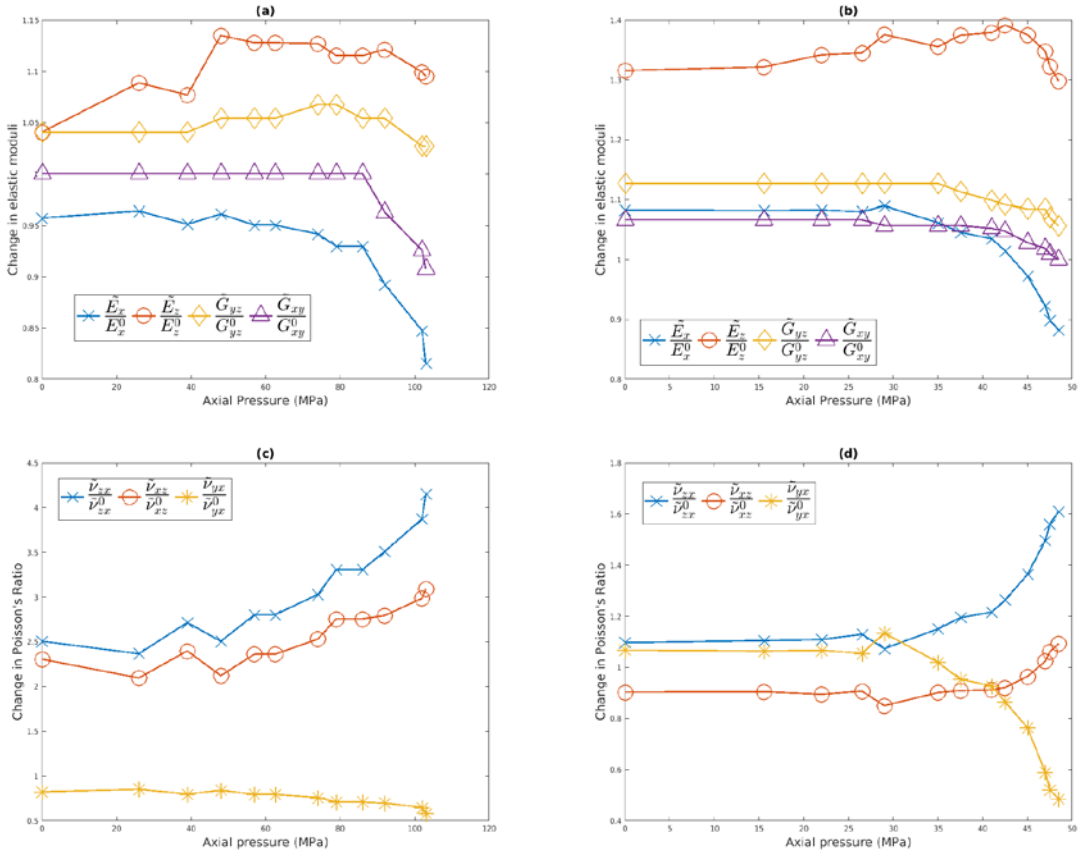

Figure 2: The corresponding change in the elastic moduli with damage for a dry (a) and wet (b) shale rock specimen under triaxial loading with a confining pressure of 15MPa for the experimental results of Sarout and Guéguen (2008a) (see Fig. 14). The corresponding change in the Poisson's ratio with damage for a dry (c) and wet (d) shale rock specimen. Their experimental results showed a change in the elastic moduli but not in the material axes of symmetry with the axis of isotropy remaining in the z direction.

Table 1: Initial elastic moduli for dry shale rock specimen in Fig. 1 and 2 for experimental results of Sarout and Guéguen (2008a) (in Table 3, room pressure results)

$E(=E_x=E_y)$	24.48GPa	$G(=G_{xy}=E/(2(1+\upsilon))$	7.40GPa
$E^t(=E_z)$	15.91GPa	$G^t(=G_{xz}=G_{yz})$	10.80GPa
$\upsilon(=\upsilon_{xy}=\upsilon_{yx})$	0.3183		
$\upsilon^t(=\upsilon_{zx}=\upsilon_{zy})$	0.0678		
$\upsilon_{xz}\,(=\upsilon_{yz})$	0.1213		

Table 2: Initial elastic moduli for wet shale rock specimen in Fig. 1 and 2 for experimental results of Sarout and Guéguen (2008a) (in Table 3, room pressure results)

$E(=E_x=E_y)$	27.25GPa	$G(=G_{xy}=E/(2(1+\upsilon))$	10.50GPa
$E^t(=E_z)$	17.21GPa	$G^t(=G_{xz}=G_{yz})$	7.10GPa
$\upsilon(=\upsilon_{xy}=\upsilon_{yx})$		0.2976	
$\upsilon^t(=\upsilon_{zx}=\upsilon_{zy})$		0.2198	
$\upsilon_{xz}(=\upsilon_{yz})$		0.3480	

perimental results of Sarout and Guéguen (2008a) (see Fig. 14). The axial pressure was applied in the z direction, and the shale was initially transverse isotropic with an axis of isotropy in the z direction. From symmetry considerations we can deduce that the lowest symmetry that should result from triaxial loading (axial stress applied in the z direction) of a transverse isotropic solid with axis of isotropy in the z direction is transverse isotropic with the same material axes in the undamaged and damaged state. The experimental results of Sarout et al. (2007); Sarout and Guéguen (2008a) confirmed this assumption and the ultrasonic measurements of the elastic wave velocities showed a change in the elastic moduli but not in the material axes of symmetry with the axis of isotropy remaining in the z direction.

Similarly to our previous paper (Olsen-Kettle (2018)) we observe that the damage tensors in Fig. 1 are not diagonal using the principal stress directions as the model coordinates. Often only a subset of the diagonal elements of the damage tensor are retained (see for example Gaede et al. (2013); Chow and Wang (1987); Lemaitre et al. (2000)) and the principal directions of a second order or fourth order anisotropic damage tensor are assumed to coincide with the applied principal stress directions (Chow and Wang (1987)). However we show that the off-diagonal elements of the fourth order damage tensor are nonzero using the principal stress directions as our model axes.

In Fig. 2(a) and (b) we observe that $\tilde{E}^t = \tilde{E}_z$ increases due to strain hardening from microcrack closure perpendicular to the compressive axial stress in the z direction for the lower values of axial pressure applied in the experiments of Sarout and Guéguen (2008a). As the shale reaches its peak axial stress and failure localizes along a shear band inclined at approximately 45° to the bedding plane (Sarout and Guéguen (2008a)), we observe that E_z begins to decrease with rupture of the shale. We observe that $\tilde{E} = \tilde{E}_x(=\tilde{E}_y)$ decreases due to microcracking parallel to the compressive axial stress in the z direction which then progress to macrocracking and rupture localization

along a shear band inclined at approximately 45° to the bedding plane.

For the variation in Poisson's ratio in Fig. 2(c) and (d) we observe that the wet and dry samples show slightly different overall qualitative behaviour and this could be partly attributed to their different initial elastic moduli in Tables 1 and 2. First we can analyze the variation in Poisson's ratio in Fig. 2(c) and (d) for the lower axial pressures where the confining pressure of 15MPa has a dominant effect. Tables 1 and 2 show that the highest Poisson's ratio for the dry shale sample is $\upsilon = \upsilon_{yx} = 0.3183$ and for the wet shale sample it is $\upsilon_{xz} = 0.3480$. When a material is subject to a constant confining pressure of 15MPa in the experiments of Sarout and Guéguen (2008a) in Fig. 2 when the axial stress is zero, a high anisotropic Poisson's ratio, υ_{ij}, means that a confining pressure in direction i will cause extension in direction j becoming more compressible in this direction and thus υ_{ij} decreases for initially high values of anisotropic Poisson's ratio. Conversely for a low anisotropic Poisson's ratio, υ_{ij}, a confining pressure in direction i will cause very little extension in direction j and the material accommodates the deformation without changing shape thus becoming less compressible in this direction and υ_{ij} increases for initially low values of anisotropic Poisson's ratio. This explains qualitatively why υ_{yx} decreases for the dry shale and υ_{xz} decreases for the wet shale, while the remaining Poisson's ratio for the respective samples increase for a constant confining pressure for the wet shale. Sarout *et al.* also confirmed this observation that elastic anisotropy decreases with both isotropic and axial stress applied perpendicular to the rock bedding plane.

We can also analyze the variation in Poisson's ratio in Fig. 2(c) and (d) for the highest axial pressures where the samples have reached peak axial stress and have ruptured. Once the samples have ruptured and the strain has localized onto a shear band the deformation is accommodated by the shear rupture plane. This means that υ_{zx} increases as the axial load in z direction no longer causes extension the x-y plane as the vertical microcracks close and the deformation is accommodated by the rupture plane (Kuila et al. (2011)), thus it becomes less compressible in the x-y planes and $\upsilon_{zx} (= \upsilon_{zy})$ increases.

Because Sarout *et al.* only considered normal stresses in the direction of the material axes we expect that there is no shear coupling with respect to the material axes in the elastic regime. This means that the applied normal stresses result in normal strains only and thus the effect on the shear moduli is relatively small until rupture of the specimen occurs as shown in Fig. 2(a) and (b).

Table 3: Initial elastic moduli for Uniflo® polyester composite of Marguéres and Meraghni (2013) in Fig. 3

$E(=E_x=E_y)$	8.82GPa	$G(=G_{xy}=E/(2(1+\upsilon))$	3.00GPa
$E^t(=E_z)$	8.02GPa	$G^t(=G_{xz}=G_{yz})$	2.65GPa
$\upsilon(=\upsilon_{xy}=\upsilon_{yx})$		0.4702	
$\upsilon^t(=\upsilon_{zx}=\upsilon_{zy})$		0.2756	
$\upsilon_{xz}(=\upsilon_{yz})$		0.2504	

Table 4: Initial elastic moduli for the glass fibre-reinforced composite of Castellano et al. (2017) in Fig. 4

$E(=E_x=E_y)$	10.93GPa	$G(=G_{xy}=E/(2(1+\upsilon))$	7.98GPa
$E^t(=E_z)$	31.78GPa	$G^t(=G_{xz}=G_{yz})$	2.23GPa
$\upsilon(=\upsilon_{xy}=\upsilon_{yx})$		-0.3152	
$\upsilon^t(=\upsilon_{zx}=\upsilon_{zy})$		0.2622	
$\upsilon_{xz}(=\upsilon_{yz})$		0.0902	

5.2. Damage induced anisotropy in composite samples

Figures 3(a) and 4(a) plot the internal tensorial damage variables for two composite samples for the experimental results using a polyester composite specimen (see Marguéres and Meraghni (2013) Table 6, column 3) and for the experimental results using a glass fibre-reinforced composite specimen (see Castellano et al. (2017) Table 2). It is somewhat more difficult to interpret the results for the experimental loading conditions of Marguéres and Meraghni (2013) and Castellano et al. (2017) as they used both sample geometries and experimental boundary and loading conditions which may not preserve the transverse isotropic symmetry of the composite samples being investigated. Another complicating factor in analyzing their results is that both experiments subjected their composite specimen to a localized low velocity impact which produced localized areas of damage and indentation even for low velocity impact (Marguéres and Meraghni (2013); Castellano et al. (2017)). There should be some caution in interpreting their results for measured elastic velocities at the macroscale for the whole specimen. Because

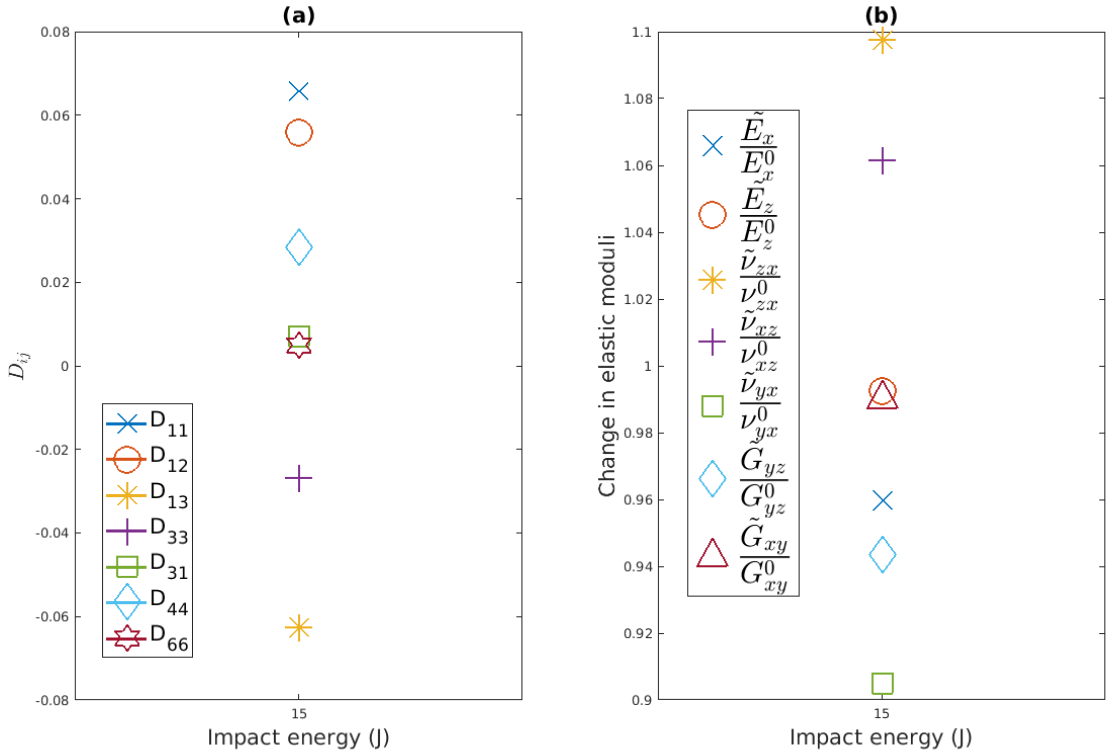

Figure 3: (a) The internal tensorial damage variables for a polyester (Uniflo®) composite subject to a low-velocity impact with energy 15J in the z direction with an impact diameter of 25mm for the experimental results of Marguéres and Meraghni (2013) (Table 6, column 3). The composite was clamped at the ends in the x direction. (b) The corresponding change in the elastic moduli with damage. Their experimental results showed a change in the elastic moduli but not in the material axes of symmetry with the axis of isotropy remaining in the z direction.

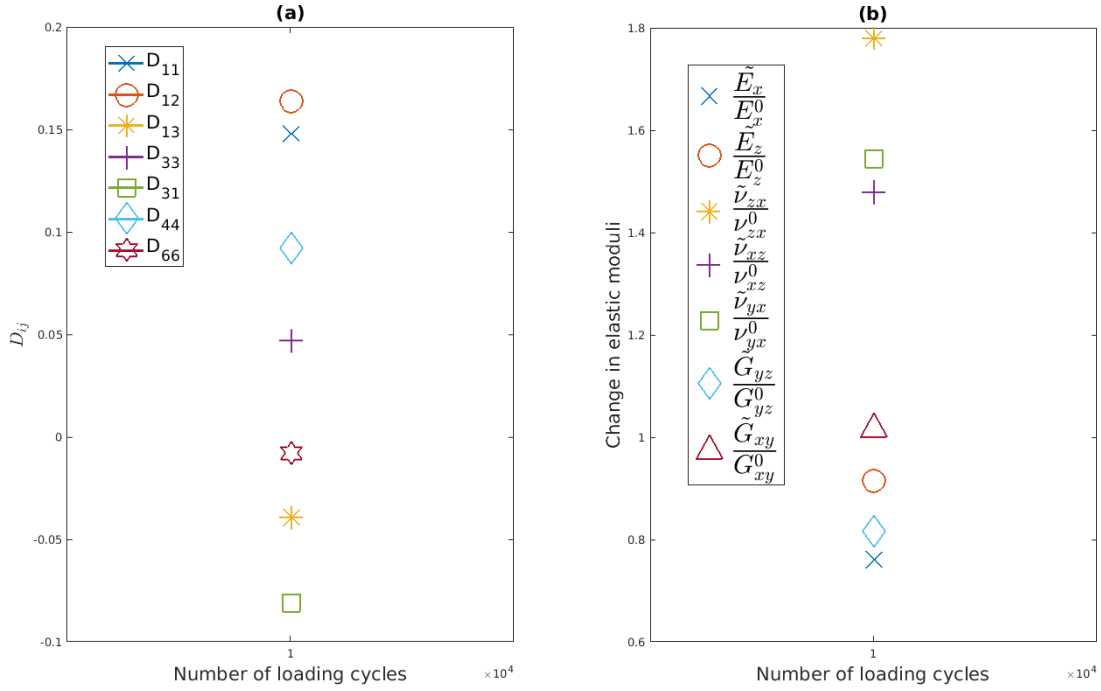

Figure 4: (a) The internal tensorial damage variables in for the fatigue post low-velocity impact test for a glass fibre-reinforced composite for the experimental results of Castellano et al. (2017) (Table 2). The composite was first subject to a low-velocity impact with energy 7J in the x direction and then subsequent fatigue tensile loading in the z direction. (b) The corresponding change in the elastic moduli with damage. Their experimental results showed a change in the elastic moduli but not in the material axes of symmetry with the axis of isotropy remaining in the z direction.

of the impact the damage is localized and moderately diffuse and it would be expected that the elastic velocities may vary spatially within the sample, however the measurements of the elastic velocities and densities are assumed for the whole specimen.

Castellano et al. (2017) subjected a thin, rectangular composite to a low-velocity impact with energy 7J and impact diameter of 10mm in the x direction and then subsequent fatigue tensile loading in the z direction. Marguéres and Meraghni (2013) subjected a thin rectangular composite (dimensions 250mm×50mm×3.6mm) to a low-velocity impact with energy 15J and impact diameter of 25mm in the z direction. The composite was clamped at the ends in the x direction. It is expected that with these respective boundary and loading conditions, and the specimen geometries, that the initial transverse isotropic symmetry may be broken during impact or loading. However both Castellano et al. (2017) and Marguéres and Meraghni (2013) showed that due to the very low impact energies imposed it caused moderately diffuse damage and that the damage induced anisotropy resulted in a change of the degree of anisotropy of the material, but not in a change of its symmetry class or material symmetry axes. Both showed that the composites remained transverse isotropic with the same material axes with loading.

We see again that the damage tensor is not diagonal in Fig. 3(a) and 4(a) using the principal stress directions as the model coordinates. It is little more difficult to interpret the single ultrasonic velocity measurements in Fig. 3 and 4 because they only contain one measurement and it is hard to visualize the progression of the elastic moduli with damage as we could in Fig. 1 and 2.

Interpreting the damaged elastic moduli is more straightforward in Fig. 3 for the experimental results of Marguéres and Meraghni (2013) where they only consider a low velocity impact in the z direction for a polyester composite. The impact in the z direction caused some extension in the x-y plane and a subsequent reduction in E_x (and E_y). Because the composite is very thin in the z direction the impact possibly caused not just compression in the z direction at the impact but also out-of-plane bending in the z direction and thus extension in this direction also. As we mentioned because the measurements are at the macroscale we cannot identify localized regions where the elastic moduli may change at the mesoscale and we see that E_z remains relatively constant.

Similarly to the analysis of Sarout *et al.'s* results for Poisson's ratio we observe that the Poisson's ratio became less anisotropic under loading in Fig. 3(b). We observe that the highest Poisson ratio $\upsilon_{yx}(= 0.4702)$ decreases

after the impact while the two lower Poisson's ratios increase. The impact in the z direction is likely to have most effect on the shear moduli in the x-z and y-z plane, with a decrease in the shear modulus $G_{yz}(= G_{xz})$ as observed in Fig. 3(b).

Castellano *et al.*'s results are much less straightforward and it is possible that the impact loading in the x direction may have broken the transverse symmetry in the x-y plane. Another complicating factor in their experiments is that the impact loading and subsequent tensile loading caused visible damage in the impact region and a fracture in the z direction near the gripping area (see Castellano et al. (2017), Fig. 8(b)). Possibly because of this fracture in the z direction we observe that the Young's modulus decreases most for $E_x(= E_y)$, and that E_z also decreases due to tensile loading in the z direction in Fig. 4(b).

The impact in the x direction is likely to have most effect on the shear moduli in the x-z and x-y plane affecting the shear modulus G_{xz} and G_{xy}. Table 4 shows that initially the shear moduli G_{xz} is more than 3.5 times lower than G_{xy}, potentially meaning that G_{xz} is much more affected and decreases substantially after loading as observed in Fig. 4(b).

A very interesting result in Fig. 4(b) is that υ_{zx} and υ_{yx} become more anisotropic under loading. This could possibly be attributed to the fact that initially $\upsilon_{yx} = -0.3152$ is negative. Fig. 4(b) shows that υ_{zx} increases becoming more positive while υ_{yx} decreases becoming more negative. This could possibly be explained by the fact that the tensile load in the z direction causes contraction in the x-y plane due to the fact that $\upsilon_{zx} > 0$. The contraction in the x (or y) direction cause further contraction in the y (or x) direction due to the fact that $\upsilon_{yx} < 0$, creating a positive feed-back effect which may lead to these values becoming more anisotropic.

6. Conclusions and future work

We have developed models of anisotropic damage for initially transverse isotropic materials undergoing damage-induced anisotropy to remain transverse isotropic with the degree of anisotropy changing but not the material symmetry axes. In section 4.2 we quantified the relationship between the internal damage variables of a fourth rank transverse isotropic damage tensor in terms of the empirical damage parameters given by ultrasonic measurements. We extend upon the seminal work of Cauvin and Testa (1999a,b) who considered anisotropic damage for initially isotropic undamaged solids, and

the work of Jarić et al. (2012) who considered initially isotropic and cubic undamaged solids. In this paper we consider anisotropic damage for initially transverse isotropic solids. We expanded the analysis of Cauvin and Testa (1999a,b) to relate the evolution of the internal fourth order anisotropic damage tensor to experimentally measured stiffness reduction of initially transverse isotropic solids undergoing anisotropic damage. We chose this measure of damage as ultrasonic investigations are widely used and provide a convenient experimental tool to measure the evolution of the full stiffness tensor with damage.

We provide an alternative phenomenological approach to quantifying anisotropic 3D damage for transverse isotropic materials using continuum damage mechanics. In contrast to previous work based on micromechanical approaches (Mallet et al. (2013, 2014); Sarout and Guéguen (2008b)) we employ an ap- proach based on continuum damage mechanics to relate the general fourth rank tensorial damage variables defined using continuum damage mechanics to ultrasonic measurements of initially transverse isotropic materials undergoing damage-induced anisotropy to remain transverse isotropic. This work can help validate and develop models of anisotropic damage using continuum damage mechanics which until now have been unable to be experimentally validated.

Other researchers (Audoin and Baste (1994); Hufenbach et al. (2006); Castellano et al. (2017)) have also identified purely phenomenological models of anisotropic damage for composite materials. Our approach defines the damage tensor differently to these purely phenomenological models which use a simple definition of damage relating to the stiffness tensor reduction. We employ the conventional definition for a tensorial damage tensor given by continuum damage mechanics (Cauvin and Testa (1999a); Jarić et al. (2012)) for the internal damage tensor in this paper. We define a relationship between the measured stiffness reduction and the internal tensorial damage variables given by continuum damage mechanics. This work paves the way to build physically based continuum damage models of anisotropic damage evolution. Future work will extend upon these models of transverse isotropic damage resulting from well-defined and constrained loading experiments which result in transverse isotropic damage at both the meso and macroscale level to modelling localized damage at the mesoscale level.

Analysis of the experimental results of Sarout and Guéguen (2008a); Castellano et al. (2017) and Marguéres and Meraghni (2013) have shown that both the loading conditions and initial values of the anisotropic elastic

moduli are important in determining damage-induced anisotropy in initially anisotropic materials. Poisson's ratio was affected the most in all the experiments. We saw in the analysis of the results of Castellano et al. (2017) that the sign of the anisotropic Poisson's ratio is also important in interpreting the experimental results.

This research is supported by the Australian Research Council Discovery Early Career Researcher Award DE140404398.

Audoin, B., Baste, S., 1994. Ultrasonic evaluation of stiffness tensor changes and associated anisotropic damage in a ceramic matrix composite. J. Appl. Mech. 61, 309.

Baste, S., Aristiégui, C., 1998. Induced anisotropy and crack systems orientations of a ceramic matrix composite under off-principal axis loading. Mech. Mat. 29, 19.

Bažant, Z., 1984. Microplane model for strain-controlled inelastic behavior. In: Desai, C., Gallagher, R. (Eds.), Mechanics of engineering materials. Wiley, Ch. 3, pp. 45–59.

Bažant, Z., Caner, F., 2005. Microplane model m5 with kinematic and static constraints for concrete fracture and anelasticity. i: Theory. J. Eng. Mech. 131, 31.

Bonnelye, A., Schubnel, A., David, C., Henry, P., Guglielmi, Y., Gout, C., Fauchille, A.-L., Dick, P., 2017. Elastic wave velocity evolution of shales deformed under uppermost crustal conditions. J. Geophys. Res. Solid Earth 122, 130.

Caner, F., Bažant, Z., 2013. Microplane model M7 for plain concrete. 1: Formulation. J. Eng. Mech. 139, 1714.

Castellano, A., Fraddosio, A., Piccioni, M., 2017. Ultrasonic goniometric immersion tests for the characterization of fatigue post-lvi damage induced anisotropy superimposed to the constitutive anisotropy of polymer composites. Composites Part B 116, 122.

Cauvin, A., Testa, R., 1999a. Damage mechanics: basic variables in continuum theories. Int. J. Solids Structures 36, 747–761.

Cauvin, A., Testa, R., 1999b. Elastoplastic material with isotropic damage. Int. J. Solids Structures 36, 727–746.

Cazcu, O., Soare, S., Kondo, D., 2007. On modelling the interaction between initial and damage-induced anisotropy in transversely isotropic solids. Math. Mech. Solids 12, 305.

Chaboche, J., 1993. Development of continuum damage mechanics for elastic solids sustaining anisotropic and unilateral damage. Int. J. Damage Mech. 2, 311–329.

Chow, C., Wang, J., 1987. An anisotropic theory of elasticity for continuum damage mechanics. Int. J. Fracture 33, 3–16.

Dodds, K., Dewhurst, D., Siggins, A., Ciz, R., 2007. Experimental and theoretical rock physics research with application to reservoirs, seals and fluid processes. J. Pet. Sci. Eng. 57, 16–36.

Gaede, O., Karrech, A., Regenauer-Lieb, K., 2013. Anisotropic damage mechanics as a novel approach to improve pre- and post-failure borehole stability analysis. Geophys. J. Int. 193, 1095–1109.

Guéguen, Y., Kachanov, M., 2011. Effective elastic properties of cracked rocks - an overview. In: Leroy, Y., Lehner, F. (Eds.), Mechanics of Crustal Rocks. CISM Courses and Lectures, Ch. 533, pp. 73–125.

Halm, D., Dragon, A., Charles, Y., 2002. A modular damage model for quasi-brittle solids interaction between initial and induced anisotropy. Archive Appl. Mech. 72, 498.

Hufenbach, W., Böhm, R., Langkamp, A., Kroll, L., Ritsche, T., 2006. Ultrasonic evaluation of anisotropic damage in multiaxially textile reinforced themoplastic hybrid composites made by hybrid yarns. Mech. Composite Mat. 42, 151.

Jarić, J., Kuzmanović, D., Šumarac, D., 2012. On anisotropic elasticity damage mechanics. Int. J. Damage Mech. 22, 1023–1038.

Ju, J., 1990. Isotropic and anisotropic damage variables in continuum damage mechanics. J. Eng. Mech. 116, 2764.

Kuila, U., Dewhurst, D., Siggins, A., Raven, M., 2011. Stress anisotropy and velocity anisotropy in low porosity shale. Tectonophysics 503, 34.

Lemaitre, J., 1996. A course on damage mechanics. Springer-Verlag.

Lemaitre, J., Desmorat, R., Sauzay, M., 2000. Anisotropic damage law of evolution. European Journal of Mechanics, A/Solids 19, 187–208.

Mallet, C., Fortin, J., Guéguen, Y., Bouyer, F., 2013. Effective elastic properties of cracked solids: an experimental investigation. Int. J. Fracture 182, 275.

Mallet, C., Fortin, J., Guéguen, Y., Bouyer, F., 2014. Evolution of the crack network in glass samples submitted to brittle creep conditions. Int. J. Fracture 190, 111.

Marguéres, P., Meraghni, F., 2013. Damage induced anisotropy and stiffness reduction evaluation in composite materials using ultrasonic wave transmission. Composites: Part A 45, 134–144.

Murakami, S., 1988. Mechanical modeling of material damage. J. Appl. Mech. Trans. ASME 55, 280–286.

Murakami, S., 2012. Continuum damage mechanics A Continuum Mechanics Approach to the Analysis of Damage and Fracture. Springer.

Olsen-Kettle, L., 2018. Bridging the macro to mesoscale: Evaluating the fourth order anisotropic damage tensor parameters from ultrasound measurements of an isotropic solid under triaxial stress loading, in press, Int. J. Damage Mechanics.

Paterson, M., Wong, T.-F., 2005. Experimental Rock Deformation - The Brittle Field. Springer-Verlag.

Piane, C. D., Almqvist, B. S., MacRae, C. M., Torpy, A., Mory, A. J., Dewhurst, D. N., 2015. Texture and diagenesis of ordovician shale from the canning basin, western australia: Implications for elastic anisotropy and geomechanical properties. Mar. Petrol. Geol. 59, 56.

Sarout, J., Guéguen, Y., 2008a. Anisotropy of elastic wave velocities in deformed shales. Part I: Experimental results. Geophysics 73, D75–D89.

Sarout, J., Guéguen, Y., 2008b. Anisotropy of elastic wave velocities in deformed shales. Part II: Modeling results. Geophysics 73, D91–D103.

Sarout, J., Molez, L., Guéguen, Hoteit, N., 2007. Shale dynamic properties and anisotropy under triaxial loading: Experimental and theoretical investigations. Phys. Chem. Earth 32, 896–906.

Sayers, C., Kachanov, M., 1995. Microcrack-induced elastic wave anisotropy of brittle rocks. J. Geophys. Res. 100(B3), 4149–4156.

Voyiadjis, G., Kattan, P., 2006. Damage mechanics with fabric tensors. Mechanics of Advanced Materials and Structures 13, 285.

Voyiadjis, G., Kattan, P., 2009. A comparative study of damage variables in continuum damage mechanics. I. J. Damage Mechanics 18, 315.

Voyiadjis, G., Kattan, P., 2012. A new class of damage variables in continuum damage mechanics. J. Eng. Mat. Tech. 134, 021016.

Yang, Q., Leng, K., 2014. A microplane-based anisotropic damage effective stress. I. J. Damage Mechanics 23, 178.

Zhu, W., Tang, C., 2004. Micromechanical model for simulating the fracture process of rock. Rock Mech. Rock Eng. 37, 25–56.